Lowpower fast wave antenna loading as a radiofrequency sheath diagnostic

D. A. D'Ippolito and J. R. Myra

Citation: Physics of Plasmas (1994-present) **3**, 420 (1996); doi: 10.1063/1.871813
View online: http://dx.doi.org/10.1063/1.871813
View Table of Contents: http://scitation.aip.org/content/aip/journal/pop/3/1?ver=pdfcov
Published by the AIP Publishing

Low-power fast wave antenna loading as a radio-frequency sheath diagnostic

D. A. D'Ippolito and J. R. Myra
Lodestar Research Corporation, Boulder, Colorado 80301

(Received 9 August 1995; accepted 12 September 1995)

Radio-frequency (RF) sheaths induced by the RF $E_\parallel$ component are a ubiquitous feature of Ion Cyclotron Range of Frequency (ICRF) heating and current drive. An important consequence of RF sheaths is the power dissipation, $P_{\rm sh}$, caused by ions accelerated in the rectified sheath potential and flowing into material boundaries, such as the antenna structure and nearby limiters. It is shown that the RF sheath-power dissipation yields an antenna loading resistance R_L larger than the usual fast wave (FW) loading at very low RF power $P_{\rm RF}$ (typically below 100 kW), because $P_{\rm sh}$ scales as $|E_{\rm rf}|$, whereas the FW coupled power scales as $|E_{\rm rf}|^2$. The curve $R_L(P_{\rm RF})$ has a maximum at $P_{\rm RF}=0$ and rapidly decreases with power until asymptoting at the usual FW loading. The ratio $R_L(0)/R_L(\infty)$ is a measure of the average RF sheath voltage on the antenna and nearby limiter surfaces. It is suggested that this technique could be used to measure the RF sheath properties of different antennas or operational regimes (e.g., different phasings) before attempting high-power operation. A generalized loading model is applied to interpret recent measurements on the DIII-D tokamak [*Plasma Physics and Controlled Nuclear Fusion Research 1990* (International Atomic Energy Agency, Vienna, 1991), Vol. I, p. 69] for a four-strap antenna with and without a Faraday screen. The possible use of this effect as a diagnostic for the scrape-off layer density is also discussed. © *1996 American Institute of Physics.* [S1070-664X(96)00401-1]

I. INTRODUCTION

It is by now well established that high-power Ion Cyclotron Range of Frequency (ICRF) antenna systems can heat fusion plasmas over a wide range of operational regimes, and ICRF systems are also being developed for driving steady-state current in tokamaks. An important development in support of these applications is the recent progress in our understanding of ICRF–edge plasma interactions, and in our ability to control unwanted effects such as ICRF-specific impurity generation (see Ref. 1 for a recent review). It was suggested that radio-frequency (RF) sheaths, studied originally in RF probe theory,[2] occur at the surfaces of the antenna and nearby limiters during high-power ICRF heating and current drive and are the mechanism behind RF-specific impurity generation.[3–7] Detailed modeling[8–11] of the Joint European Torus (JET)[12] and Tokamak Fusion Test Reactor (TFTR)[13] has shown that RF-enhanced sputtering models can account for the measured impurity influxes from the Faraday screen (FS) under a wide variety of conditions. RF sheaths can also cause other measured scrape-off-layer (SOL) modifications such as enhanced radial convection,[14–16] SOL density depletion,[17] and stochastic electron heating.[18] Diagnosis and control of RF sheath interactions are necessary to achieve good heating efficiency and fault-free antenna operation at high power and to minimize perturbation of the SOL plasma. In support of this goal, a computer code called ANSAT (ANtenna Sheath Analysis Tool) has been developed to compute the spatial RF sheath voltage distribution for realistic antenna geometries.[19] It is also very important to develop direct experimental measurements of the dependence of the RF sheath voltage distribution on the antenna and plasma parameters.

The purpose of this paper is to suggest a diagnostic of the RF sheath distribution on fast-wave (FW) antennas and, possibly, of the SOL density itself; the diagnostic is based on the measurement of the low-power (<100 kW) antenna loading. This idea was stimulated by recent experimental data[20] from the DIII-D tokamak,[21] in which the low-power antenna loading plotted as a function of RF power showed significantly different structure during ICRF antenna operation with and without a FS. Since minimization of RF sheath effects is an important aspect of ICRF antenna design and operation (as discussed below), it would be very useful to have available a sheath diagnostic that perturbed the SOL plasma as little as possible while testing the antennas.

The essential physics of RF sheaths can be summarized as follows.[2–6] The voltage driving the sheaths is given by $V_{\rm rf}=\int ds\, E_\parallel$, where $E_\parallel$ is the component of the RF electric field parallel to **B**, and is induced by the mismatch of the equilibrium magnetic field with the antenna structure. When plasma of sufficient density is present on field line segments intersecting the antenna, the electron response to $E_\parallel$ shorts out the electric field over most of the field line segment, leaving sheaths of positive space charge and intense electric fields near the contact points. To confine electrons and maintain quasineutrality (time averaged over a RF cycle), $V_{\rm rf}$ is "rectified"[2–6] by the sheath to produce a steady-state voltage $V_0(x,y)$ on each field line. The magnitude of V_0 depends on the antenna and magnetic field geometry, the current-strap phasing, and scales with RF power as $(P_{\rm RF})^{0.5}$ at fixed electron density n_e. If $V_{\rm rf}$ is defined to be the zero-to-peak voltage, the rectified potential at high density (full space charge) is given in the limit $eV_{\rm rf}/T_e \gg 1$ by $V_0 \approx 0.6\, V_{\rm rf}$.[6] The spatial variation of the rectified voltage $V_0(x,y)$ drives **E×B** convection[16] in the SOL, and ions accelerated in the sheaths give rise to enhanced sputtering of FS and limiter impurities.[4–9] Here and elsewhere in this paper, we use

 1070-664X/96/3(1)/420/7/$6.00

(x,y,z) to denote the radial, poloidal, and toroidal directions, respectively.

For the present work, the most important sheath effect is that ions are accelerated in the sheath potential before they strike the material surface, thereby transferring energy to it from the RF fields; this represent a power loss to the RF system. In the limit $eV_{\rm rf}/T_e \gg 1$, this ''sheath-power dissipation'' is given by[9] the product of the ion flux $(n_i c_s)$, the energy gain $(\mathrm{Ze}\,V_0)$, and the surface area covered by the sheaths normal to **B** summed over both contact points $(2A_n)$, i.e.

$$P_{\rm sh} = 1.9\times 10^{-16} Z n_i (ZT_e/\mu)^{1/2} V_{\rm rf} A_n , \tag{1}$$

where the units of $P_{\rm sh}$, A_n, n_i, T_e, and V are kW, cm^2, cm^{-3}, eV, and V, respectively. Throughout this paper, all RF voltages, e.g. the sheath driving voltage $V_{\rm rf}$ and the antenna voltage V_a, will be specified as zero-to-peak values. We have written Eq. (1) assuming a single ion species of charge Ze and mass $\mu=(m_i/m_p)$, and the relation $c_s=(ZT_e/m_i)^{1/2}$ was used for the ion parallel velocity at the entrance to the sheath in the limit $ZT_e \gg T_i$, consistent with the Bohm sheath condition, as derived in Ref. 22. Without repeating the derivation, one can motivate the Z dependence of c_s by noting that the single-fluid parallel momentum flow in the presheath is balanced by the total parallel pressure gradient; assuming a single ion species the change in velocity across the presheath is roughly given by $\Delta u^2 \approx (n_e T_e + n_i T_i)/(n_i m_i) = (ZT_e + T_i)/m_i$ using quasineutrality $(n_e = Z n_i)$. The generalization of c_s to multiple ion species is straightforward.[23]

Equation (1) can be integrated over the surface area of the antenna to obtain the total dissipated power caused by the RF sheaths. The power dissipation can also be calculated from a lumped-circuit model of the antenna; there is a nonzero RF current I associated with the RF voltage V and a power dissipation given by the time-averaged $\langle VI\rangle$ of the equivalent circuit. In the Appendix, we describe a simple model that illustrates the equivalence of this calculation with Eq. (1) in the large-$V_{\rm rf}$ limit. The circuit model is used in Sec. II to generalize Eq. (1) to the regime $eV_{\rm rf}/T_e < 1$.

The importance of RF sheath-power dissipation was demonstrated in a high-power ICRF experiment at JET in which large RF sheath voltages were obtained by reversing the direction of the tokamak toroidal field.[9] (This increased the mismatch between the B field and the FS bars, which were slanted in the direction of the normal B field direction.) With monopole (0–0) phasing of the antenna current straps, the RF sheath voltages were maximized[7] and the heating efficiency was observed to drop by 40% in reversed-field operation, consistent with the theoretical estimate of the RF sheath-power dissipation.[9]

Another way of viewing this effect is by analogy to an RF probe.[5,24] The RF probe model was used by Greene in unpublished work to explain his low-power loading measurements for a variety of antennas in a small research tokamak.[24] For several unshielded antennas, he measured a large-density-dependent loading resistance that he attributed to a ''particle collection effect,'' essentially the sheath-power dissipation given in Eq. (1). For his shielded antennas, a much smaller loading resistance was measured, which had spikes at the location of wave resonances. We would like to point out that Greene's measurements clearly demonstrate the basic principle that the sheath-power dissipation is sensitive to the details of the antenna design. This point was illustrated again by the recent low-power antenna loading measurements on DIII-D during ICRF operation with and without a FS.[20] The DIII-D data showed an increase in the antenna loading below an RF power of about 50 kW; the effect was large (more than a factor of 3) when the FS was removed, but was much smaller when the screen was present. An increase in the low-power loading has also been observed on other tokamaks.[25,26]

The plan of this paper is as follows. A simple model is given in Sec. II, which illustrates the contribution of the sheath-power dissipation $P_{\rm sh}$ to the low-power antenna loading R_L. In Sec. III we compute the shape of the antenna loading curve $R_L(P_{\rm RF})$ and investigate its dependence on the sheath voltage distribution and on the local plasma density. The relevance of this model to the DIII-D measurements is also discussed. Section IV contains a brief summary.

II. THE MODEL

The power coupled to the core plasma via the fast wave, $P_{\rm FW}$, and the power dissipated in the RF sheaths are independent loss channels driven by the antenna current. Thus, the lumped circuit resistances of these two channels are taken in series, and the antenna loading resistance R_L can be expressed as

$$R_L = \frac{2(P_{\rm FW}+P_{\rm sh})}{(V_a/Z_0)^2}, \tag{2}$$

where V_a is the antenna voltage and Z_0 is the antenna impedance. The power radiated into the FW is approximated by $P_{\rm FW} = A_{\rm FS}\, S_x$, where $A_{\rm FS} = L_y L_z$ is the antenna surface area, $S_x = c^2 \eta |E_y|^2/(8\pi\omega)$ is the Poynting flux, and η is the antenna surface impedance (see below). The voltage scaling for the FW power coupling is $S \propto |E_y|^2 \propto V_a^2$, with $|E_y| \approx V_a/L_y$. For the sheath-power dissipation, Eq. (1) implies that $P_{\rm sh}$ scales linearly with the sheath driving voltage $V_{\rm rf}$ in the limit $eV_{\rm rf}/T_e \gg 1$, and $V_{\rm rf}$ is directly proportional to the antenna voltage, so $P_{\rm sh} \propto V_a$. Another RF power dissipation mechanism, scattering of short-wavelength modes excited by the FS periodicity, has recently been investigated[27] and the dissipated power calculated to scale as $V_a^{5/2}$. We have neglected it in Eq. (2) because, with this voltage scaling, it affects the shape of the loading curve only at high RF power. At very low RF power, or equivalently low V_a, these scalings imply that the dominant power loss mechanism is the sheath-power dissipation. Equation (2) implies the scalings $R_L \propto V_a^{-1} \propto P_{\rm RF}^{-1/2}$ at low power, where $P_{\rm sh} > P_{\rm FW}$, and $R_L \approx$ const at higher RF power, where $P_{\rm FW}$ gives the dominant contribution (see Fig. 1). This behavior is qualitatively similar to the recent DIII-D antenna loading data.[20] (The apparent singularity as $P_{\rm RF} \to 0$ is resolved below.) It will be shown in Sec. III that the magnitude and width of the low-power loading peak is sensitive to the details of the RF

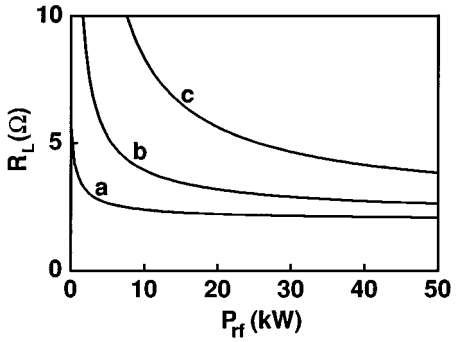

FIG. 1. Antenna loading versus RF power for $n_i=10^{11}$ cm^{-3} and three values of the RF sheath voltage parameter $\alpha\equiv V_{\rm rf}/V_a$: (a) $\alpha=0.05$, (b) $\alpha=0.2$, and (c) $\alpha=0.5$. The large increase in loading as $P_{\rm RF}\rightarrow 0$ is caused by power dissipation in the RF sheaths.

sheath physics and can therefore be used as a sheath diagnostic for comparison of different RF operating regimes with the same antenna.

To establish the physical basis for our proposed diagnostic, we describe how to calculate these effects quantitatively for comparison with experimental loading measurements. It is straightforward to generalize Eq. (1) to include the low-power limit, $eV_{\rm rf}/T_e\rightarrow 0$. To do this self-consistently, one would have to compute $P_{\rm sh}$ and R_L numerically using a code such as the one described in Ref. 6. An analytic result can be obtained using the two-point model described in the Appendix. In this model, the antenna potential at the two points of contact between a field line and the antenna surface is assumed to vary as $V_{1,2}=\pm V_{\rm rf}\cos(\omega t)-V_0$, where the plasma is assumed to be at zero potential, $V_{\rm rf}$ is the sheath driving voltage, and the rectified voltage V_0 is calculated from the requirement of zero time-averaged current drawn by the antenna. The power dissipation $P_{\rm sh}=\langle (V_1-V_2)I\rangle$ is computed from the equivalent lumped-parameter circuit, with I defined as the current through the circuit. Making use of the result of this calculation [Eq. (A8)], Eq. (1) is replaced by

$$P_{\rm sh}=6.2\times 10^{-16} Z n_i (ZT_e/\mu)^{1/2} V_{\rm rf} A_n h(\xi)\,\frac{I_1(\xi)}{I_0(\xi)}, \qquad (3)$$

where $\xi=eV_{\rm rf}/T_e$ and $h(\xi)=(0.5+0.3\xi)/(1+\xi)$ is a form factor that adjusts the two-point model to give the correct numerical coefficient in the large-ξ limit. Eq. (3) is the desired generalization of Eq. (1) to treat the small-ξ limit in which $P_{\rm sh}\propto\xi^2$ and R_L approaches a finite value. It is shown in the Appendix [Eq. (A13)] that the sheath power dissipation is dominated by ions accelerated in the sheaths for large ξ, but it has both electron and ion contributions in the limit of small ξ.

Equation (3) can be applied separately on each field line using the local values of density, temperature, sheath voltage, and projected area, and the result integrated over the antenna to obtain the total dissipated power. This is easily done using the ANSAT code.[19] While this procedure would be appropriate in carrying out data analysis in an experiment, here we employ a simpler procedure. For the present purpose, it is sufficient to use typical values of the parameters in Eq. (3): we interpret n_i as the ion density averaged over all field lines with RF sheaths (which we approximate as the average density in the private SOL of the antenna), $A_n\approx\Delta x\ L_y$, with Δx denoting the radial extent of the private SOL which is covered by RF sheaths, and T_e is the local electron temperature. The sheath driving voltage is estimated as $V_{\rm rf}=\alpha V_a$, where α depends on the magnetic field and antenna geometry, the current strap phasing, etc., as discussed in Sec. IV.

As suggested above, the power coupled to the core plasma by the FW can be estimated analytically using the Poynting flux as $P_{\rm FW}=A_{\rm FS}S_x\upsilon=A_{\rm FS}c^2\eta\upsilon|E_y|^2/(8\pi\omega)$, where $\omega=2\pi f$ with f the RF frequency and η is the antenna surface impedance. The proportionality constant υ is related to the antenna geometry and to density profile effects on the loading (such as the location of the fast wave cutoff). The factor υ can be evaluated with suitable FW loading codes[28,29] and is typically less than unity, but in this paper we set $\upsilon=1$ for simplicity. Note that $A_{\rm FS}=L_yL_z$ is the area of the FS projected normal to the antenna surface, whereas the relevant area A_n in the sheath-power dissipation formula is the projected area normal to the magnetic field lines. For cases where the FW is cut off near the antenna, the antenna surface impedance $\eta\equiv{\rm Im}\,(E_y^{-1}\,\partial E_y/\partial x)$ can be calculated in terms of Bessel's functions using a simple model given in the Appendix of Ref. 16. Here, we restrict the discussion to the case where the FW is propagating at the antenna (which is true, for example, in the limit of small $k_\parallel$). In this case, local theory is applicable ($\eta\rightarrow k_x$), and we can approximate $k_x\approx\omega_{pi}/c$ using the FW dispersion relation with both the density and the RF fields evaluated at the antenna. Finally, the average RF field can be approximated as $|E_y|\approx V_a/L_y$ to obtain

$$P_{\rm FW}=10^{-4}\,\frac{\upsilon n_i^{1/2}V_a^2}{f}\,\frac{L_z}{L_y}, \qquad (4)$$

where the units of L, n_i, f, and V_a are cm, cm^{-3}, MHz, and kV, respectively. Equation (4) contains the scaling $P_{\rm FW}\propto V_a^2$ required to understand the experimental loading curve.

III. NUMERICAL EXAMPLES

The antenna loading resistance, given by Eqs. (2)–(4), depends on some parameters that are typically known (the antenna geometry, voltage and impedance, RF frequency, etc.) and others that need to be calculated or measured (the sheath voltage and projected area, the local plasma density, and temperature). In this section, we illustrate the dependence of the low-power loading curve on the sheath driving voltage $V_{\rm rf}$ and on the local ion density n_i in the private SOL of the antenna. The tendency toward RF sheath formation will be parametrized by the parameter $\alpha=V_{\rm rf}/V_a$, and we keep in mind the scaling $V_{\rm rf}\propto V_a\propto P_{\rm RF}^{1/2}$. The other parameters are chosen to have values similar to those on DIII-D with a deuterium plasma: $f=60$ MHz, $Z_0=30\ \Omega$, $L_z=1$ m, $L_y=0.5$ m, $\Delta x=4$ cm, $T_e=20$ eV, $\mu=2$, and $Z=1$.

In Fig. 1, we show the curve $R_L(P_{\rm RF})$ for $n_i=10^{11}$ cm^{-3} and three levels of sheath formation, $\alpha=0.05$, 0.2, and 0.5. (The correspondence of these parameters with operating modes of the antenna will be discussed below.) Figure 1 illustrates the general shape of the loading curve: R_L has a

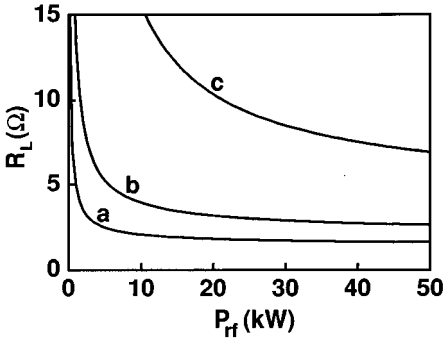

FIG. 2. Antenna loading versus RF power for $\alpha \equiv V_{rf}/V_a = 0.2$ and three values of the local ion density at the antenna: (a) $n_i = 5\times10^{10}$ cm^{-3}, (b) $n_i = 10^{11}$ cm^{-3}, and (c) $n_i = 2\times10^{11}$ cm^{-3}. The large increase in loading as $P_{RF}\to 0$ is due to power dissipation in the RF sheaths.

(finite) maximum at $P_{RF}=0$ caused by the sheath-power dissipation and asymptotes to a constant value characteristic of the high-power FW coupling as $P_{RF}\to\infty$. The threshold power P_t where the loading curve has a ''knee'' (i.e., the FW and sheath contributions to R_L are comparable) generally occurs at very low power ($P_t < 25$ kW for most cases studied) and increases with α. An important point illustrated by Fig. 1 is that the magnitudes of the quantities $R_L(0)/R_L(\infty) \equiv R_L(P_{RF}\to 0)/R_L(P_{RF}\to\infty)$ and P_t increase rapidly with α and therefore serve as good diagnostics of the RF sheath voltage averaged over the antenna and nearby limiter surfaces.

As explained in Sec. II, the low-power peak in the loading occurs because of the different voltage scalings, $P_{sh}\propto P_{RF}^{1/2}$ vs $P_{FW}\propto P_{RF}$. This effect can explain the shape of the loading curve without invoking RF-induced density profile changes, such as RF convection[16] or ponderomotive density expulsion. In fact, nonlinear modifications of the density profile are extremely small for FW antennas at such low powers. The role of density profile effects was tested in a recent analysis of the DIII-D data.[30] Antenna loading calculations were carried out using the standard FW coupling theory with the density profiles near the antenna obtained from microwave reflectometer measurements. The conclusion of this study was that the measured density profile changes with RF could not account for the extremely high loading measured at low power for the DIII-D screenless antenna experiment.[30]

Although small changes in the density profile shape do not significantly affect the loading, there is an explicit dependence of both P_{sh} and P_{FW} on the overall magnitude of the density [see Eqs. (3) and (4)]. This dependence of R_L on local ion density is illustrated in Fig. 2. The three loading curves correspond to the densities $n_i = 5\times10^{10}$, 1×10^{11}, and 2×10^{11} cm^{-3} for $\alpha=0.2$. It can be seen that the asymptotic values of both the sheath loading (as $P_{RF}\to 0$) and the FW loading (as $P_{RF}\to\infty$) are sensitive to the ion density near the antenna. Both $R_L(0)/R_L(\infty)$ and P_t increase rapidly, with n_i at fixed α. This suggests that the low-power loading curve could also be used as a density diagnostic by comparing the shape of the curves calculated for different density values with the measured loading curve.

Finally, it is interesting to apply these results qualitatively to illustrate why one would expect different low-power loading curves with and without a Faraday screen in the recent DIII-D experiments.[20,30] A simple analytic antenna model will be used here for purposes of illustration;[7] more detailed numerical calculations, taking into account the full antenna geometry, are possible using the ARGUS–ANSAT antenna codes.[19] The analytic model assumes a poloidally uniform current along the current straps, neglects feeder contributions to the RF magnetic flux driving the sheaths, and in its original form assumed two current straps per antenna. For antennas with N straps ($N>2$), it is convenient to express V_{rf} in terms of the voltage drive per current strap, V_1, i.e.,

$$V_{rf} = \kappa V_1 \equiv \frac{\kappa L_z}{N L_y}\tan\theta\ V_a\,, \tag{5}$$

where (L_z/N) and L_y are the toroidal and poloidal dimensions of the antenna structure corresponding to each strap, θ is the B-field misalignment angle in the poloidal–toroidal plane, and $\kappa = V_{rf}/V_1$ is the RF sheath enhancement factor for a typical field line passing in front of the N-strap antenna.

The parameter κ is estimated as follows. Assuming that a typical field line links the RF magnetic flux of N current straps and that each strap gives an equal contribution to the sheath voltage, it can be shown that $\kappa = \kappa_N \equiv \sin(N\,\Delta\phi/2)/\sin(\Delta\phi/2)$, where $\Delta\phi$ is the phase difference between current straps. For a four-strap antenna of the DIII-D type, this estimate yields $0 \leqslant \kappa_4 \leqslant 4$, depending on the antenna phasing: $\kappa_4 = 4$ for monopole phasing ($\Delta\phi = 0$), whereas $\kappa_4 = 0$ for dipole phasing ($\Delta\phi = \pi$) and current drive phasing ($\Delta\phi = \pi/2$). When the details of the antenna and magnetic geometry are taken into account in numerical calculations,[19] one finds that the typical field line intersecting the antenna does not pass in front of all the current straps and thus the flux cancellation is never perfect. For example, the sheath enhancement factor for a field line passing in front of only two current straps in current drive phasing ($\Delta\phi = \pi/2$) is $\kappa = \kappa_2 \approx 1.4$. (The flux cancellation is further reduced when finite-antenna and corner effects are taken into account.) For the present calculation, we will use $\kappa = 1.5$ as a conservative estimate of the sheath enhancement factor (averaged over all field lines) for the DIII-D antenna in $(0, \pi/2, \pi, 3\pi/2)$ phasing. Substituting this value of κ and the geometric parameters used in Figs. 1 and 2 into Eq. (5), we obtain the result $\alpha \equiv V_{rf}/V_a = 0.75\tan\theta$.

In estimating α, one difference between antenna operation with and without a FS is modeled by the choice of θ. With a FS, the misalignment angle θ is defined as the angle between the FS bars and the equilibrium magnetic field, because the FS acts to polarize the RF field perpendicular to its bars. Without a FS, the fast wave RF field is polarized in the direction of the current straps (perpendicular to the toroidal direction) and θ is defined as the inclination angle of the equilibrium magnetic field with respect to the toroidal direction. We model the DIII-D loading data[20] by the values $\theta = 4°$ and $\kappa = 1.5$ ($\Rightarrow \alpha = 0.05$) for operation using a FS with nearly field-aligned bars and $\theta = 15°$ and $\kappa = 1.5$ ($\Rightarrow \alpha = 0.2$) for operation without a FS. Thus, the lowest curve in Fig. 1 depicts the calculated loading for normal operation with a FS, whereas the middle curve in Fig. 1 describes operation with-

out a screen. These two curves are qualitatively consistent with the important features of the DIII-D data. In particular, note the very small enhancement of the loading as $P_{RF} \rightarrow 0$ during normal operation with the FS, whereas a more than threefold enhancement is predicted for screenless operation. The top curve in Fig. 1 ($\alpha = 0.5$) is the model calculation for a ''worst-case'' situation: the DIII-D antenna in 0–0–0–0 phasing ($\kappa = 4$) without a FS ($\theta = 15°$).

While the qualitative agreement described above is encouraging, additional factors need to be considered to obtain a definitive explanation of the DIII-D data. These include the contribution of feeder-driven RF sheaths[19] and the local density change when the FS is removed.[20] The quantitative analysis of these effects is deferred to future work.

IV. SUMMARY

In this paper, we have described a candidate physical process (RF sheath-power dissipation) to explain the ubiquitous increase in ICRF antenna loading at low RF power. A simple model was given in Sec. II for calculating the contribution of the sheath-power dissipation to the low-power antenna loading, and an analytic sheath model was given in the Appendix to elucidate the sheath power balance for arbitrary eV_{rf}/T_e. In Sec. III, numerical calculations were carried out to illustrate the typical size of the sheath loading, and it was shown how to apply the theory to the recent DIII-D comparison of screened and screenless antennas.[20]

The main point of this paper is that the sensitivity of the low-power FW antenna loading to the sheath voltage distribution and to the local density at the antenna suggests exploring its possible use as an antenna and SOL diagnostic. The recent experimental work[20] on DIII-D shows that the antenna loading can be calibrated down to the 1–10 kW level, and the model calculations of the present paper suggest that the resulting measurements have a simple physical interpretation in terms of RF sheath physics. The ability to accurately determine the density profile in front of the antenna by microwave reflectometry[31] makes possible, in principle, very accurate calculations of the sheath-power dissipation using the ANSAT code.[19] More experimental work and detailed theoretical modeling will be needed to assess the usefulness of this effect as a diagnostic.

ACKNOWLEDGMENTS

We would like to thank R. Pinsker, D. Swain, M. Bures, S. Golovato, and Y. Takase for helpful conversations concerning FW antenna loading measurements. We are also grateful to R. Pinsker for informing us of G. Greene's experimental work and sending us a copy of the relevant material in Greene's thesis during the writing of this paper.

This work was supported by the U.S. Department of Energy (DOE) under Contract No. DE-FG02-88ER53263; however, this support does not constitute an endorsement by DOE of the views expressed herein.

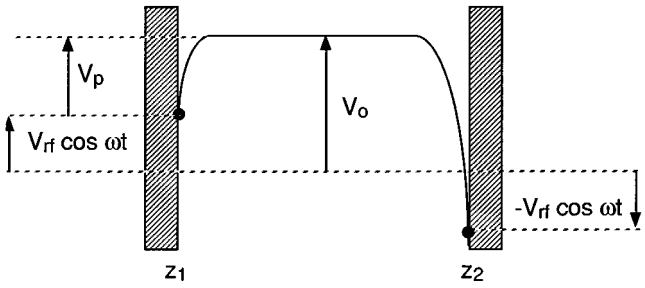

FIG. 3. Plasma-filled capacitor model of an RF sheath.

APPENDIX: DERIVATION OF SHEATH POWER DISSIPATION

In this appendix we present a model of power dissipation in an RF sheath. The model, while simple, has several features critical to the present paper: (i) it allows the computation of an effective loading that is nonsingular for all powers; (ii) it presents an intuitive picture of energy balance in the sheath; and (iii) it is fully analytic.

We consider a plasma-filled, parallel plate capacitor model with sheaths at each end, as illustrated in Fig. 3. The potentials at the left and right plates (respectively located at z_1 and z_2) relative to the plasma potential are

$$V_1 = V_{rf}\cos(\omega t) - V_0, \quad V_2 = -V_{rf}\cos(\omega t) - V_0, \tag{A1}$$

where V_0 is the (time-averaged) plasma potential and $V_0 \approx 3T_e$ in the absence of an applied RF voltage. Considering initially one sheath (e.g., at $z = z_1$), the potential of the plasma relative to the plate is

$$V_p = V_0 - V_{rf}\cos(\omega t) > 0. \tag{A2}$$

To calculate the electron current to the left plate, we assume the electron distribution function is Maxwellian and integrate over that portion of the leftgoing tail with $mv^2/2 > |e|V_p$ to obtain

$$J_{e1} = -(2\pi)^{-1/2} n_e e v_e \exp(-eV_p/T_e). \tag{A3}$$

The ions can be in either the jitter regime or the immobile regime,[6] depending on parameters; in the present case we consider the immobile ion limit when the frequency is too fast to elicit a significant inertial response. In this case

$$J_{i1} = Z n_i e u, \tag{A4}$$

where $u \approx c_s = (ZT_e/m_i)^{1/2}$ is the flow velocity of ions into the sheath (the Bohm sheath condition). Summing over the sheaths at both ends and demanding

$$\langle J \rangle = \langle J_e + J_i \rangle = 0, \tag{A5}$$

where $\langle\ \rangle$ is a time average over the wave period, yields the rectified (zero-frequency) voltage of the plasma

$$x_0 \equiv \frac{eV_0}{T_e} = x_B + \ln[I_0(\xi)], \tag{A6}$$

where we have defined $\xi = eV_{rf}/T_e$, $x_B = 0.5\ln(m_i/2\pi Z m_e) \sim 3$ is the Bohm sheath value of x_0 in the absence of RF, and I_0 is a modified Bessel function. For $V_{rf} = 0$, Eq. (A6) recovers the usual Bohm result $V_0 \approx 3T_e$. For $\xi \gg 1$, the as-

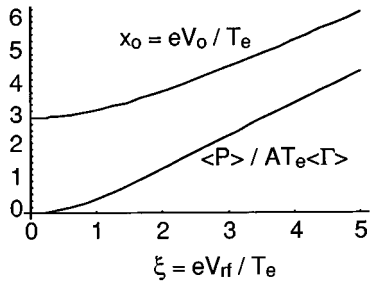

FIG. 4. Functional dependences of the rectified potential V_0 and the dissipated power $\langle P\rangle$ in an RF sheath. Note that at low power $\langle P\rangle \propto \xi^2 \propto P_{\mathrm{RF}}$, implying that the sheath contribution to the antenna loading is finite.

ymptotic result is $eV_0 \sim eV_{\mathrm{rf}} - (T_e/2)\ln(2\pi eV_{\mathrm{rf}}/T_e) + 3T_e$, which differs from the true result by a numerical factor of order unity,[6] viz., typical numerical results of a fully self-consistent one-dimensional model show that $V_0 \sim CV_{\mathrm{rf}}$ with $C \sim 0.6$.

The power dissipation in the sheaths is readily calculated from the above model by treating the entire plasma-filled capacitor as a circuit element. The total current flowing *through* the capacitor is

$$I = \frac{A}{2}\frac{n_e e v_e}{(2\pi)^{1/2}}\left[\exp\left(\frac{eV_1}{T_e}\right) - \exp\left(\frac{eV_2}{T_e}\right)\right], \tag{A7}$$

where A is the area of all sheaths, i.e. $A/2$ is the area of one of the plates. Thus, the dissipated power in the sheaths is

$$\begin{aligned}\langle P\rangle &= \langle (V_1 - V_2)I\rangle \\ &= (2/\pi)^{1/2} A n_e e v_e V_{\mathrm{rf}} \exp(-x_0) I_0'(\xi), \\ &= A\langle\Gamma\rangle T_e \xi I_1(\xi)/I_0(\xi),\end{aligned} \tag{A8}$$

where $I_0'(\xi) = dI_0(\xi)/d\xi$. The last form of Eq. (A8) is obtained by noting that the time-averaged particle flux into the plates, $\langle\Gamma\rangle \equiv \langle\Gamma_i\rangle \equiv \langle\Gamma_e\rangle$, is

$$\langle\Gamma\rangle = \frac{n_e v_e}{(2\pi)^{1/2}} \exp(-x_0) I_0(\xi) = Z n_i c_s . \tag{A9}$$

Finally, we note that for asymptotically large V_{rf}, we have $\langle P\rangle \sim A(n_i c_s)(\mathrm{Z}\, V_{\mathrm{rf}})$, which has the simple interpretation that it is just the power delivered to the plates by ions falling down a rectified potential of size $V_0 \sim V_{\mathrm{rf}}$ [Eq. (A6)]. The functional dependence of the rectified potential and the dissipated power are shown in Fig. 4.

Equation (A8) is the desired expression for the sheath-power dissipation; however, it is pedagogically useful to proceed one step further and develop an energy balance relation for power flow in the sheath. To this end, we note that the instantaneous electron heat flux to the plates, H_e, may be derived in a manner analogous to the particle flux,

$$\Gamma_e = \int_{v_p} dv_\parallel\, v_\parallel f_{\mathrm{M}} = (2\pi)^{-1/2} n_e v_e \exp\left(\frac{-eV_p}{T_e}\right), \tag{A10}$$

$$H_e = \int_{v_p} dv_\parallel\, v_\parallel \left(\frac{mv^2}{2}\right) f_{\mathrm{M}} = \Gamma_e(2T_e + eV_p), \tag{A11}$$

where f_{M} is the Maxwellian and the integration is again over the tail particles with $mv^2/2 > |e|V_p$. Averaging H_e over an RF cycle results in

$$\langle H_e\rangle = \frac{n_e T_e v_e}{(2\pi)^{1/2}} \exp(-x_0)[(2+x_0)I_0(\xi) - I_0'(\xi)], \tag{A12}$$

from which the time-averaged sheath energy transmission factor, $\gamma_e = \langle H_e\rangle/(\langle\Gamma_e\rangle T_e)$ may be calculated. By combining the above expressions, we can construct an energy balance relation,

$$\langle H\rangle + \frac{\langle P\rangle}{A} = 2T_e\langle\Gamma_e\rangle + eV_0\langle\Gamma_i\rangle, \tag{A13}$$

where, for simplicity, we have taken the limit of $T_i = 0$, so that the ion heat flux from the presheath is negligible, $\langle H_i\rangle = 0$. Equation (A13) has the following simple interpretation: the left-hand side represents the energy sources to the sheath, viz. the heat flux flowing into the sheath from the presheath ($\langle H\rangle$) and the RF power dissipated in the sheath ($\langle P\rangle/A$); the first term on the right-hand side represents the power flow to the plates of the electrons, and the second term gives the ion contribution. Note that the right-hand side of Eq. (A13) describes the energies of the electron (ions) *at the plate*, i.e. *after* they have climbed up (fallen down) the sheath potential.

[1] J.-M. Noterdaeme, in *Proceedings of the 9th Topical Conference on Radio Frequency Power in Plasmas*, Charleston, South Carolina (American Institute of Physics, New York, 1992), p. 71.
[2] H. S. Butler and G. S. Kino, Phys. Fluids **6**, 1346 (1963).
[3] F. W. Perkins, Nucl. Fusion **29**, 583 (1989).
[4] R. Chodura and J. Neuhauser, in *Proceedings of the 16th European Conference on Controlled Fusion and Plasma Heating*, Venice (European Physical Society, Petit-Lancy, 1989) Vol. 13B, Part III, p. 1089.
[5] R. Van Niewenhove and G. Van Oost, J. Nucl. Mat. **162–164**, 288 (1989).
[6] J. R. Myra, D. A. D'Ippolito, and M. J. Gerver, Nucl. Fusion **30**, 845 (1990).
[7] D. A. D'Ippolito, J. R. Myra, M. Bures, and J. Jacquinot, Plasma Phys. Controlled Fusion **33**, 607 (1991).
[8] M. Bures, J. Jacquinot, K. Lawson, M. Stamp, H. P. Summers, D. A. D'Ippolito, and J. R. Myra, Plasma Phys. Controlled Fusion **33**, 937 (1991).
[9] M. Bures, J. Jacquinot, M. Stamp, D. Summers, D. F. H. Start, T. Wade, D. A. D'Ippolito, and J. R. Myra, Nucl. Fusion **32**, 1139 (1992).
[10] R. Majeski, D. A. D'Ippolito, Y. L. Ho, J. Hosea, S. Medley, M. Murakami, J. R. Myra, C. K. Phillips, J. H. Rogers, G. Schilling, J. Stevens, G. Taylor, J. R. Wilson, and the TFTR Group, in *Proceedings of the 20th European Physical Society Conference on Controlled Fusion and Plasma Physics*, Lisbon (European Physical Society, Petit-Lancy, 1993), Vol. 17C, Part III, p. 977.
[11] D. A. D'Ippolito, J. R. Myra, R. Majeski, and J. R. Wilson, Bull. Am. Phys. Soc. **39**, 1627 (1994), Paper 4R 17.
[12] P. H. Rebut and the JET Team, in *Plasma Physics and Controlled Nuclear Fusion Research 1990* (International Atomic Energy Agency, Vienna, 1991), Vol. I, p. 27.
[13] D. J. Grove and D. M. Meade, Nucl. Fusion **25**, 1167 (1985).
[14] R. Van Nieuwenhove, G. Van Oost, P. E. Vandenplas, R. A. Moyer, D. Gray, and R. W. Conn, Fusion Eng. Design **12**, 231 (1990); D. Bora, R. S. Ivanov, G. Van Oost, and U. Samm, Nucl. Fusion **31**, 2383 (1991).
[15] JET Team, presented by J. Jacquinot, Plasma Phys. Controlled Fusion **33**, 1657 (1991).
[16] D. A. D'Ippolito, J. R. Myra, J. Jacquinot, and M. Bures, Phys. Fluids B **5**, 3603 (1993).

[17]D. A. D'Ippolito, J. R. Myra, A. C. England, G. R. Hanson, J. B. Wilgen, J. H. Rogers, R. Majeski, G. Schilling, J. R. Wilson, and J. C. Hosea, ''Generalized theory of ICRF convection and modeling of observed density profile modifications on TFTR,'' to appear in *Proceedings of the 11th Topical Conference on Applications of Radiofrequency Power in Plasmas*, Palm Springs, CA, 17–19 May 1995 (American Institute of Physics, New York, in press).
[18]J. R. Myra, D. A. D'Ippolito, and R. Majeski, in *Proceedings of the 21st European Physical Society Conference on Controlled Fusion and Plasma Physics*, Montpellier (European Physical Society, Petit-Lancy, 1994), Vol. 18B, Part II, p. 894.
[19]J. R. Myra, D. A. D'Ippolito, and Y. L. Ho, ''ANSAT, an antenna sheath analysis tool,'' to appear in Ref. 17.
[20]R. I. Pinsker, F. W. Baity, J. S. deGrassie, C. B. Forest, H. Ikezi, M. Murakami, C. C. Petty, J. P. Squire, D. W. Swain, and the DIII-D group, ''Direct electron heating with directional fast wave launch on DIII-D,'' to appear in Ref. 17.
[21]R. D. Stambaugh and the DIII-D Team, in Ref. 12, p. 69.
[22]R. Chodura, in *Physics of Plasma–Wall Interactions in Controlled Fusion*, edited by D. E. Post and R. E. Behrisch (Plenum, New York, 1986), p. 99; see Eqs. (4.3) and (4.4).
[23]See, for example, P. C. Stangeby and G. M. McCracken, Nucl. Fusion **30**, 1125 (1990), Eq. (3.71).
[24]G. J. Greene, Ph.D dissertation, California Institute of Technology, Pasadena, CA, 1984.
[25]S. Golovato and Y. Takase (private communication, 1995).
[26]M. Bures (private communication, 1995).
[27]S. Riyopoulos, Nucl. Fusion **35**, 261 (1995).
[28]M. D. Carter, D. B. Batchelor, and D. C. Stallings, Bull. Am. Phys. Soc. **38**, 2105 (1993), Paper 9Q 13.
[29]M. Bettenhausen and J. E. Scharer, Bull. Am. Phys. Soc. **38**, 2105 (1993), Paper 9Q 14.
[30]D. W. Swain, F. W. Baity, D. B. Batchelor, S. C. Chiu, J. S. deGrassie, E. J. Doyle, G. R. Hanson, K. W. Kim, R. I. Pinsker, C. C. Petty, C. L. Rettig, and J. B. Wilgen, Bull. Am. Phys. Soc. **39**, 1649 (1994), Paper 5P 28.
[31]G. R. Hanson, A. C. England, J. B. Wilgen, F. W. Baity, D. B. Batchelor, M. D. Carter, D. J. Hoffman, M. Murakami, D. A. Rasmussen, P. M. Ryan, D. W. Swain, J. H. Rogers, J. R. Wilson, R. P. Majeski, G. Schilling, E. J. Doyle, and K. W. Kim, ''Edge density modification with rf on TFTR and DIII-D,'' to appear in Ref. 17.